

Virtual RC Damping of LCL-Filtered Voltage Source Converters with Extended Selective Harmonic Compensation

Wang, Xiongfei; Blaabjerg, Frede; Loh, Poh Chiang

Published in:
I E E E Transactions on Power Electronics

DOI (link to publication from Publisher):
[10.1109/TPEL.2014.2361853](https://doi.org/10.1109/TPEL.2014.2361853)

Publication date:
2015

Document Version
Early version, also known as pre-print

[Link to publication from Aalborg University](#)

Citation for published version (APA):
Wang, X., Blaabjerg, F., & Loh, P. C. (2015). Virtual RC Damping of LCL-Filtered Voltage Source Converters with Extended Selective Harmonic Compensation. *I E E E Transactions on Power Electronics*, 30(9), 4726 - 4737 . <https://doi.org/10.1109/TPEL.2014.2361853>

General rights

Copyright and moral rights for the publications made accessible in the public portal are retained by the authors and/or other copyright owners and it is a condition of accessing publications that users recognise and abide by the legal requirements associated with these rights.

- Users may download and print one copy of any publication from the public portal for the purpose of private study or research.
- You may not further distribute the material or use it for any profit-making activity or commercial gain
- You may freely distribute the URL identifying the publication in the public portal -

Take down policy

If you believe that this document breaches copyright please contact us at vbn@aub.aau.dk providing details, and we will remove access to the work immediately and investigate your claim.

Virtual RC Damping of LCL -Filtered Voltage Source Converters with Extended Selective Harmonic Compensation

Xiongfei Wang, *Member IEEE*, Frede Blaabjerg, *Fellow IEEE*, Poh Chiang Loh

Department of Energy Technology, Aalborg University, Aalborg 9220, Denmark
xwa@et.aau.dk, fbl@et.aau.dk, pcl@et.aau.dk

Abstract—Active damping and harmonic compensation are two common challenges faced by LCL -filtered voltage source converters. To manage them holistically, this paper begins by proposing a virtual RC damper in parallel with the passive filter capacitor. The virtual damper is actively inserted by feeding back the passive capacitor current through a high-pass filter, which indirectly, furnishes two superior features. They are the mitigation of phase lag experienced by a conventional damper and the avoidance of instability caused by the negative resistance inserted unintentionally. Moreover, with the virtual RC damper, the frequency region, within which the harmonic compensation is effective, can be extended beyond the gain crossover frequency. This is of interest to some high-performance applications, but has presently not been achieved by existing schemes. Performance of the proposed scheme has been tested in the laboratory with results obtained for demonstrating stability and harmonic compensation.

Index Terms—Active damping, stability, resonance, voltage source converters, harmonic compensation

I. INTRODUCTION

LCL filters have widely been used with grid-connected voltage source converters due to their better switching ripple attenuation and smaller volumes when compared to L filters [1]. However, the presence of LCL resonance complicates the converter control and its sensitivity to harmonics [2], which can, at times, be worsened by other paralleled converters with their own resonances [3], [4]. This challenge cannot be ignored especially with more nonlinear and electronic loads connected to the grid. In addition, if the grid voltages are distorted, they tend to cause the grid converters to generate current harmonics, which often require the use of multiple resonant controllers for selective harmonic compensation [5]. Hence, it is necessary for the converters to be controlled such that they meet grid codes with effective harmonic disturbance rejection and resonance damping.

The combined requirements of resonance damping and selective harmonic compensation are generally tough to achieve simultaneously for grid converters. The latter, in particular, demands for multiple resonant current controllers to be used [6]–[8], which in theory, are multiple control functions developed for selective harmonic compensation. They should hence not be confused with the oscillatory LCL resonance.

Both concepts (selective harmonic compensation and LCL resonance damping) must however be considered together, before an optimized solution can be developed.

Beginning with selective harmonic compensation, the design of resonant controllers for converters with L filters has presently been well documented, where it has been shown that harmonics up to the Nyquist frequency can be effectively compensated [9]–[11]. The same, however, does not apply to LCL -filtered converters, where the use of resonant controllers for compensating harmonics around the LCL resonance is particularly challenging [9]. To avoid unnecessary complications, resonant controllers for LCL -filtered converters are usually placed below the gain crossover frequency, defined by the proportional gain of the current control loop [12], [13]. The purpose is to decouple the stability of resonant controllers from the influence of the LCL resonance. Although effective, this approach has two restrictions. The first is the unintentional limitation of compensating frequency ranges of the LCL -filtered converters, as compared to the L -filtered converters, whose influence on high-performance applications are even more prominent [14], [15]. The second is a large safety margin needed for accounting grid impedance variation, which may shift the gain crossover frequency over a wide range. That shifting may cause Phase Margin (PM) of the overall control system to be reduced near the gain crossover frequency, leading to unstable harmonic compensation [13].

It is therefore of interest to extend the frequency compensation range of resonant controllers, which in theory, is possible only after damping the LCL resonance effectively. Damping of LCL resonance is particularly important for a weak grid, where grid impedance and hence LCL resonance frequency vary widely. These variations can more easily cause instability if external damping is not employed. It is therefore necessary to have external damping, where the simplest approach is to add a passive damping resistor to the LCL filter. Adding a physical resistor will however inevitably raise the total power loss [16], [17]. Active damping methods are therefore preferred, which can either be implemented by cascading digital filters in series with the current controllers [18] or feeding back additional filter variables [2], [19]–[28]. In [20] and [21], voltage across the filter capacitor has been fed back through a lead-lag filter, which upon considering the

relationship between capacitor voltage and current, is equivalent to the feedbacks of both filter capacitor voltage and current through low-pass filters. In [22], the capacitor voltage has been predicted and fed back through a high-pass filter for damping purposes. This method is equivalent to the feeding back of capacitor current through a low-pass filter, if the relationship between capacitor voltage and current is again considered.

Therefore, instead of the capacitor voltage, the capacitor current can be measured explicitly for damping purposes, where the most common is through a proportional gain [2], [23]-[28]. This feedback method has subsequently been proven to be equivalent to the addition of a virtual resistor across the filter capacitor [24]. That equivalence changes to a virtual impedance when digital sampling, computational and modulation delays are considered [25]. Identified effects of the virtual impedance include a shifting of filter resonance frequency caused by its imaginary term, and the creation of a real term which may be negative depending on the ratio of the filter resonance to control frequency [26].

The negative resistance, if introduced accidentally, will add open-loop Right-Half-Plane (RHP) poles to the control loop [25], of which the closed-loop response will then have a non-minimum phase characteristic. To mitigate the non-minimum phase behaviour, a straightforward method is to reduce the computational delay by shifting the sampling instant of the capacitor current [26]. Although simple, its implementation is susceptible to aliasing error when measuring the capacitor current. Another method is to predict the capacitor current with an observer [27] or a discrete-time derivative controller [28]. These methods provide satisfactory resonance damping even with grid impedance variation, but they do not address the interaction between active damping and harmonic compensation, which can be critical around the *LCL* resonance frequency.

The challenges identified from the literature can therefore be summarized, as follows.

- Unnecessarily constraining of harmonic compensation range by merely using the resonant controllers below the gain crossover frequency. The compensation range can in practice be extended, but the new upper limit has presently not been identified.
- Proportional active damping that may not function well when implemented digitally. This is caused by the negative resistance unintentionally introduced by the system delays. This complication and its consequent non-minimum phase characteristic of the closed-loop response have presently not been resolved fully.
- Interaction between the active damper and resonant harmonic controllers has presently not been addressed thoroughly. Most research works have focused on either of them, rather than both of them in coordination.

To address these issues holistically, this paper proposes first a virtual *RC* damper for damping *LCL* resonance robustly even with a wide grid inductance variation. Realizing the damper is relatively easy, involving only a high-pass filter added to the capacitor current feedback loop for mitigating delays. Upon

damped appropriately, the effective harmonic compensation range of the *LCL*-filtered converters can then be extended beyond the traditional gain crossover frequency through coordinated design with the *RC* damper. Related findings have been verified experimentally with results presented in a later section.

II. SYSTEM DESCRIPTION

Fig. 1 shows a three-phase grid-connected voltage source converter with an *LCL*-filter, whose parameters used for design are summarized in Table I. For simplicity, the DC-link voltage V_{dc} of the converter can be treated as constant, while its grid synchronization bandwidth can be assumed as smaller than the grid fundamental frequency to avoid unintentional low-frequency instability [29]. This structure has earlier been shown by [23] to have an inherent damping effect even when only a single control loop is used for regulating the grid current i_2 . The only condition demanded is for the *LCL* resonance frequency to be placed above one-sixth of the system control frequency $f_s/6$, which in [23], is named as the critical frequency. This region is however not attractive because of its poorer switching harmonic filtering, which in general, compromises the purpose of having a *LCL* filter [23]. Moreover, the wide variation of grid impedance in weak grids may shift the *LCL* resonance frequency in a wide spectrum across $f_s/6$, giving rise to instability if no external active damping is employed.

To illustrate where the external active damping can be inserted, Fig. 2 shows the per-phase block diagram of a typical double-loop current control scheme for the converter shown in Fig. 1. The inner filter capacitor current feedback loop is mainly for active *LCL* resonance damping, whose effect can be tuned by the active damping function $G_d(s)$. The outer grid current control loop with controller $G_c(s)$ is, on the other hand, for regulation purposes, in synchronism with the voltage at the

TABLE I
MAIN PARAMETERS OF GRID-CONNECTED CONVERTER

Symbol	Meaning	Value
V_g	Grid voltage	400V
f_1	Grid frequency	50 Hz
f_{sw}	Switching frequency	10 kHz
f_s	Sampling frequency	10 kHz
T_s	Sampling period	100 μ s
V_{dc}	DC-link voltage	800 V
L_1	Converter-side filter inductor	3.6 mH
L_2	Grid-side filter inductor	1 mH
C_f	Filter capacitor	4.7 μ F

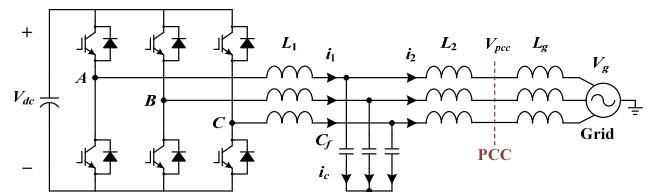


Fig. 1. A three-phase grid-connected voltage source converter with an *LCL* filter.

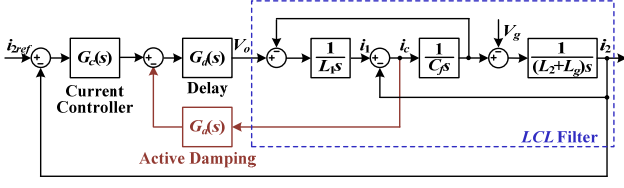


Fig. 2. Per-phase diagram of grid current control loop with external capacitor-current active damping.

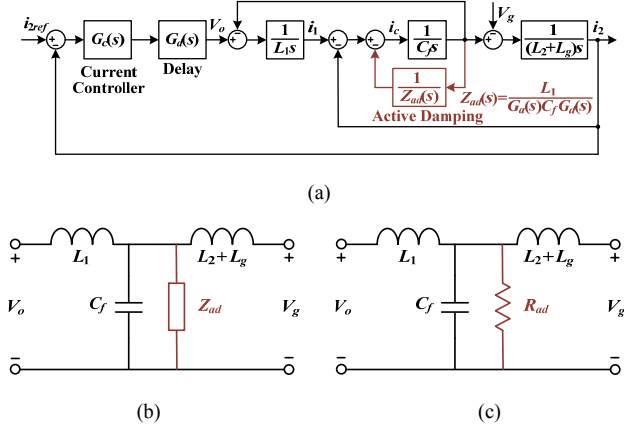


Fig. 3. Equivalent representation of capacitor-current active damping. (a) Block diagram representation. (b) Equivalent circuit with delays considered. (c) Equivalent circuit of proportional controller without considering delays.

Point of Common Coupling (PCC). Both control loops are affected by control delays, which have collectively been represented by $G_d(s)$ in (1), in terms of sampling time T_s [30].

$$G_d(s) = e^{-1.5T_s s} \quad (1)$$

To better understand the illustrated active damping, Fig. 2 has been redrawn as Fig. 3(a), which in circuit notation, represents an impedance $Z_{ad}(s)$ appearing across the filter capacitor C_f . This notation has been drawn in Fig. 3(b), which for the proportional $G_d(s)$ expressed in (2), leads to the resistive damper shown in Fig. 3(c), if delays are ignored ($Z_{ad}(s) = R_{ad}$).

$$G_d(s) = K_{ad} \quad (2)$$

With delays included, impedance $Z_{ad}(s)$ cannot be simplified, and is represented by (3) [26].

$$Z_{ad}(j\omega) = \frac{L_1}{K_{ad} C_f} [\cos(1.5\omega T_s) + j \sin(1.5\omega T_s)] \quad (3)$$

The imaginary term in (3) can, in principle, cause the *LCL* resonance frequency to vary, while its real term can become negative if the *LCL* resonance frequency is located between $f_s/6$ and the Nyquist frequency $f_s/2$. The latter implies an ineffective active damping with the non-minimum phase grid current behavior expected, owing to the presence of open-loop

RHP poles. Proportional active damping expressed in (2) is therefore not a robust solution, as compared to the proposed *RC* damper to be discussed in the following.

III. PROPOSED VIRTUAL *RC* DAMPER

A. Basic Principle

Fig. 4 shows the proposed active *RC* damper, which unlike (2), has an additional first-order high-pass filter included. The resulting transfer function can thus be expressed as (4), where K_{rc} and ω_{rc} represent its gain and cut-off frequency.

$$G_a(s) = \frac{sK_{rc}}{s + \omega_{rc}} \quad (4)$$

Corresponding equivalent circuits representing the proposed scheme can also be drawn as in Fig. 5, where a virtual series *RC* damper can clearly be seen if delays are ignored. Expressions for the damper without considering delays can specifically be derived as (5).

$$R_{rc} = \frac{L_1}{K_{rc} C_f}, \quad C_{rc} = \frac{K_{rc} C_f}{L_1 \omega_{rc}}, \quad \omega_{rc} = \frac{1}{R_{rc} C_{rc}} \quad (5)$$

These expressions change to (6) after incorporating delays.

$$\begin{aligned} Z_{rc}(j\omega) &= \frac{L_1}{K_{rc} C_f} (1 - j \frac{\omega_{rc}}{\omega}) [\cos(1.5\omega T_s) + j \sin(1.5\omega T_s)] \\ \text{Re}\{Z_{rc}(j\omega)\} &= R_{rc} \cos(1.5\omega T_s) + \frac{1}{\omega C_{rc}} \sin(1.5\omega T_s) \\ \text{Im}\{Z_{rc}(j\omega)\} &= R_{rc} \sin(1.5\omega T_s) - \frac{1}{\omega C_{rc}} \cos(1.5\omega T_s) \end{aligned} \quad (6)$$

Unlike (3) for proportional capacitor-current feedback, the real and imaginary terms of (6) include a second expression, which can be tuned by C_{rc} . This is helpful since the likelihood

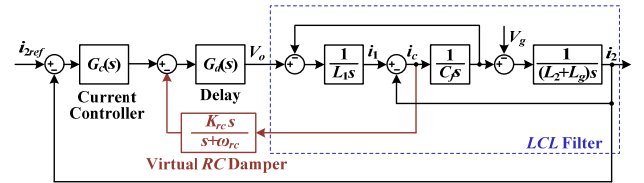


Fig. 4. Block diagram of proposed virtual *RC* damper.

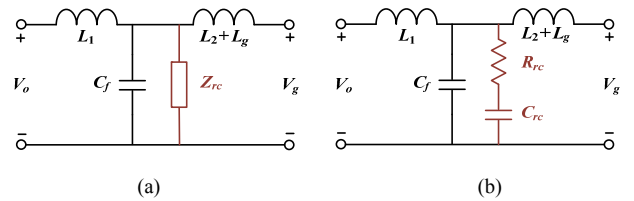


Fig. 5. Equivalent circuit of proposed virtual *RC* damper (a) with and (b) without delays considered.

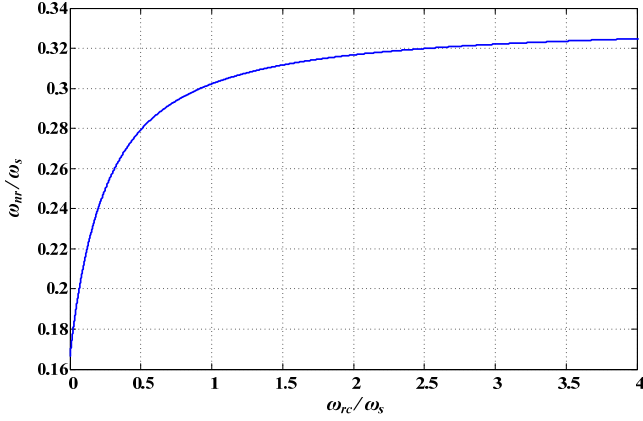


Fig. 6. Relationship between ω_{nr} and ω_{rc} .

of $\text{Re}\{Z_{rc}\}$ being negative can now be lessened by tuning. To illustrate, the frequency ω_{nr} , above which $\text{Re}\{Z_{rc}\}$ becomes negative, can be tabulated in terms of the filter cutoff frequency ω_{rc} , as shown in Fig. 6. At $\omega_{rc} = 0$, Fig. 6 also gives ω_{nr} for the proportional capacitor-current feedback scheme, which as earlier mentioned, is $\omega_{nr} = \omega_s/6 = 2\pi f_s/6$. Above $\omega_{rc} = 0$, ω_{nr} increases, which to a great extent, has demonstrated that the delay-induced phase lag has been compensated by the added high-pass filter. $\text{Re}\{Z_{rc}\}$ is thus less likely to be negative. The improvement is however not limitless, which according to Fig. 6, saturates around $\omega_{nr} = \omega_s/3$. A system with LCL resonance frequency located between $\omega_s/3$ and $\omega_s/2$ (Nyquist frequency) is therefore always burdened by the non-minimum-phase response, even with the proposed active RC damper included. It is thus a limitation of the proposed RC damper.

B. Robustness Evaluation and Parameter Tuning

For evaluating robustness subject to wide grid inductance variation, z -domain root locus analysis is performed on the scheme shown in Fig. 4. Two transfer functions of the “plant” (converter and LCL filter) are necessary, and are hence derived accordingly. The first is obtained by applying Zero-Order-Hold (ZOH) discretization to $G_{vc}(s)$ in (7) for relating the converter output voltage and filter capacitor current. The second is obtained by applying impulse invariant transformation to $G_{cg}(s)$ in (7) for relating the filter capacitor current and grid current [23]. The resulting transfer functions obtained are given in (8) and (9), where ω_{res} represents the LCL resonance frequency.

$$G_{vc}(s) = \frac{i_c}{V_o} = \frac{1}{L_1} \frac{s}{(s^2 + \omega_{res}^2)}, \quad G_{cg}(s) = \frac{i_2}{i_c} = \frac{1}{(L_2 + L_g)C_f s^2} \quad (7)$$

$$G_{vc}(z) = \frac{\sin(\omega_{res} T_s)}{\omega_{res} L_1} \frac{(z^{-1} - z^{-2})}{[z^{-2} - 2z^{-1} \cos(\omega_{res} T_s) + 1]} \quad (8)$$

$$G_{cg}(z) = \frac{T_s z^{-1}}{(L_2 + L_g)C_f (1 - z^{-1})^2} \quad (9)$$

The high-pass filter used for the virtual RC damper can next be discretized by Tustin transformation, which is expressed in (10).

$$G_a(z) = \frac{2K_{rc}(1 - z^{-1})}{(\omega_{rc}T_s - 2)z^{-1} + \omega_{rc}T_s + 2} \quad (10)$$

Combining (8) to (10), Fig. 7 shows the closed-loop pole trajectory of grid current control scheme, where $G_c(s)$ in Fig. 4 is assumed to be a simple proportional gain designed with $(L_1 + L_2)$ considered and for a PM of 45° [19]. The pole movement caused by the high-pass filter gain K_{rc} is plotted when its cut-off frequency ω_{rc} is swept from 0 to $2\omega_s$ with a step of $0.2\omega_s$. In total, three grid inductance values are evaluated with the LCL filter parameters listed in Table I, which give three resonance frequencies centered around the critical frequency of $f_s/6 = 1.67$ kHz.

Beginning with Fig. 7(a) for a resonance frequency of 2.6 kHz and $L_g = 0$ mH, it can clearly be seen that the poles mostly stay within the dashed unit circle. This is due to the inherent resonance damping effect brought by placing the resonance frequency above the critical frequency. In contrast, Fig. 7(b) and (c) show the poles initially out of the unit circle, since their resonance frequencies are smaller than $f_s/6$, and hence do not exhibit inherent damping. The poles will however track back within the unit circle as K_{rc} increases, implying stability. In addition, Fig. 7 shows that with $\omega_{rc} = 0$ or the proportional capacitor-current damping, the upper limit of K_{rc} is much reduced since ω_{nr} (see Fig. 6) is much smaller, and hence closer to the LCL resonance frequency. Where necessary, ω_{rc} should hence be increased to raise ω_{nr} , before the upper limit of K_{rc} can be increased.

In conclusion, the design of the virtual RC damper should proceed by selecting an appropriate ω_{rc} that will give an appropriate margin between the LCL resonance frequency and ω_{nr} according to Fig. 6. Root locus plots shown in Fig. 7 can then be drawn for choosing the appropriate gain K_{rc} for the high-pass filter.

C. Frequency-Domain Comparison

To further strengthen attractiveness of the proposed virtual RC damper, comparison among the three representative cases is performed in the frequency domain. As mentioned in Subsection III (B), $G_c(s)$ in Fig. 2 for all three cases has been simplified to a proportional gain designed with $(L_1 + L_2)$ and a PM of 45° considered [19]. Beginning with the first case having no external active damping ($G_a(s) = 0$ in Fig. 2), Fig. 8 shows its frequency responses when its open-loop transfer function $i_2/(i_{2ref} - i_2)$ is plotted. The plots clearly show a reduction of LCL resonance frequency as the grid inductance increases, which will eventually lead to instability when the resonance frequency falls below $f_s/6$.

With proportional capacitor-current damping $K_{ad} = 15$ added, Fig. 9 shows the redrawn Bode plots, whose different phase characteristics indicate the presence of non-minimum phase behavior. This behavior is, as explained, caused by the

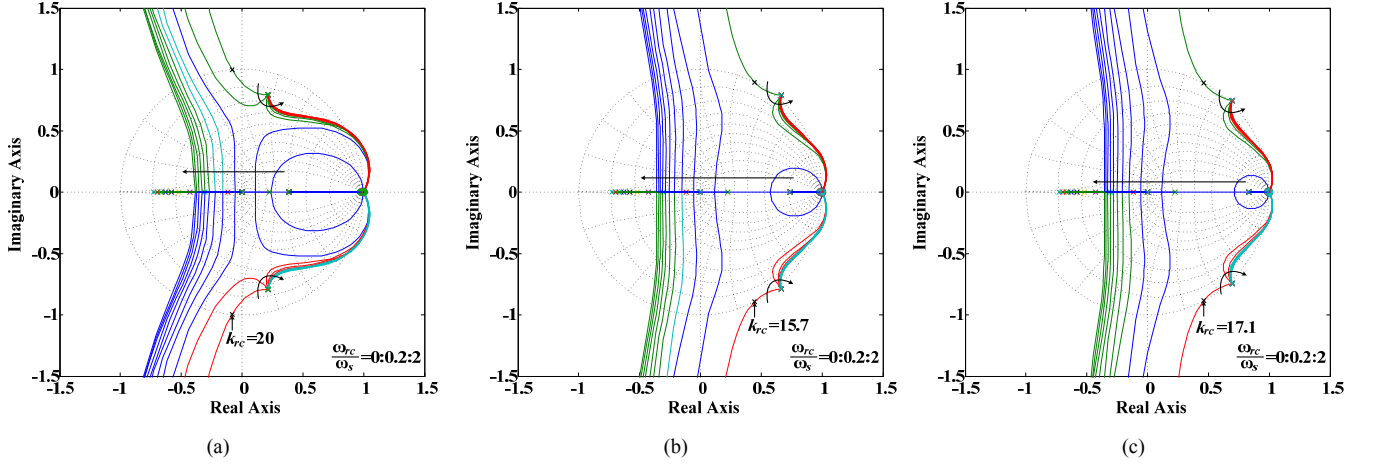


Fig. 7. Root loci of the grid current control loop obtained with different grid inductances. (a) $L_g = 0$ mH, $f_{res} = 2.6$ kHz. (b) $L_g = 4.5$ mH, $f_{res} = 1.57$ kHz. (c) $L_g = 9$ mH, $f_{res} = 1.42$ kHz.

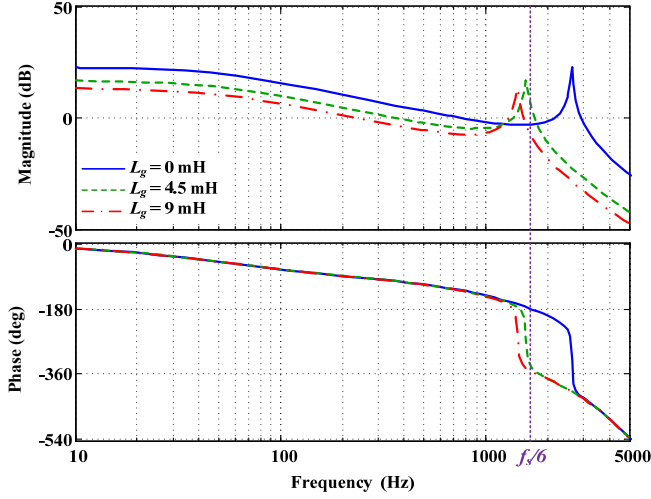


Fig. 8. Bode plots showing open-loop responses of the grid current control scheme without external active damping.

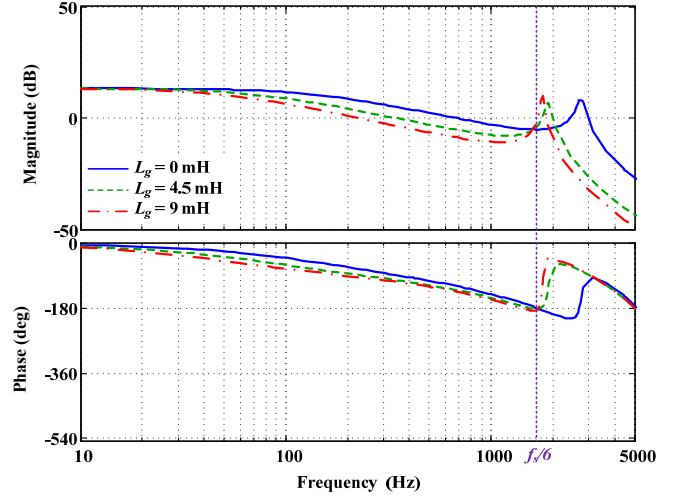


Fig. 9. Bode plots showing open-loop responses of the grid current control scheme with the conventional proportional capacitor-current active damping.

inserted negative virtual resistance. Apart from that, the resonance peaks have been reduced with their frequencies shifted slightly by the imaginary virtual term derived in (3). The studied Bode plots have again been redrawn in Fig. 10 after introducing the proposed virtual RC damper with $K_{rc} = 15$ and $\omega_{rc} = 0.2\omega_s$. The figure clearly shows that non-minimum phase behavior has been mitigated by the added virtual capacitor. Moreover, the resonant peaks have been well damped for $L_g = 4.5$ mH and $L_g = 9$ mH, whereas for $L_g = 0$ mH, the resonance frequency is shifted much higher than the critical frequency of $f_s/6$. Collectively, these observations prove the effectiveness of the proposed virtual RC damper.

D. Synchronous-Frame Implementation

The active RC damper in (4) can equivalently be realized in the synchronous frame after applying the necessary frequency-shifting transformation according to the first expression in (11) [6], [8]. Transfer function of the resulting RC damper in the synchronous frame is thus given by the second expression in (11), whose implementation involves cross-coupling, and is

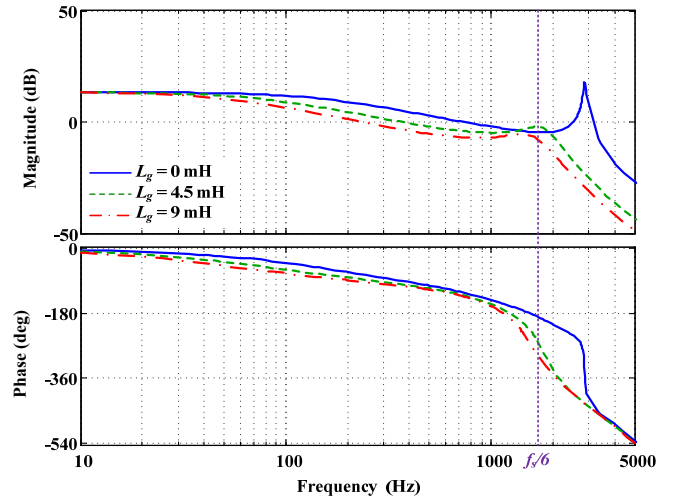


Fig. 10. Bode plots showing open-loop responses of the grid current control scheme with the proposed virtual RC damper.

hence more complex like shown in Fig. 11. Realizing and

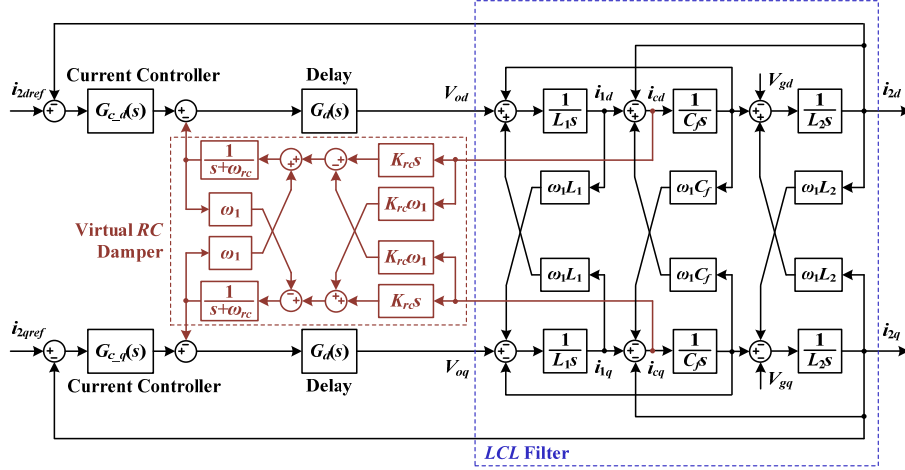


Fig. 11. Block diagram of proposed virtual RC damper in the synchronous frame.

analyzing the damper in the stationary frame is thus generally recommended because of simplicity.

$$G_{dq}(s) \Rightarrow G_{\alpha\beta}(s + j\omega_1), \quad G_{a_dq}(s) = \frac{s + j\omega_1}{s + j\omega_1 + \omega_{rc}} K_{rc} \quad (11)$$

IV. SELECTIVE HARMONIC COMPENSATION

Selective harmonic compensation is performed by placing resonant peaks at frequencies identified for compensation. It can be performed in the synchronous or stationary frame. For the latter, multiple resonant controllers are commonly used, which for L -filtered converters, have been proved to compensate for harmonics up to the Nyquist frequency [9]-[11], after introducing the necessary discretization and phase compensation. The resulting discretized resonant controllers are described next, before discussing how their harmonic compensation frequency range should be chosen for LCL -filtered converters.

A. Discretized Resonant Controllers

Fig. 12 shows two discretized resonant controllers used for selective harmonic compensation. In common, they consist of a forward Euler and a backward Euler integrator, which for the basic structure shown in Fig. 12(a), can be expressed as (12), where K_{ih} is the resonant gain, θ_h is the compensation phase lead, h is the harmonic order, and ω_l is the grid angular frequency.

$$G_{Rh}(z) = K_{ih} T_s \frac{z^{-1} [\cos(\theta_h) - h\omega_l T_s \sin(\theta_h)] - z^{-2} \cos(\theta_h)}{1 - 2z^{-1} (1 - h^2 \omega_l^2 T_s^2 / 2) + z^{-2}} \quad (12)$$

Equation (12) is, in fact, an approximation of the more precise resonant controller expressed in (13) [10]. The approximation helps to speed up computation, but is generally less accurate because of a reorientation of resonant poles and zeros from their intended positions. This discrepancy leads to frequency errors of the resonant peaks, which will further

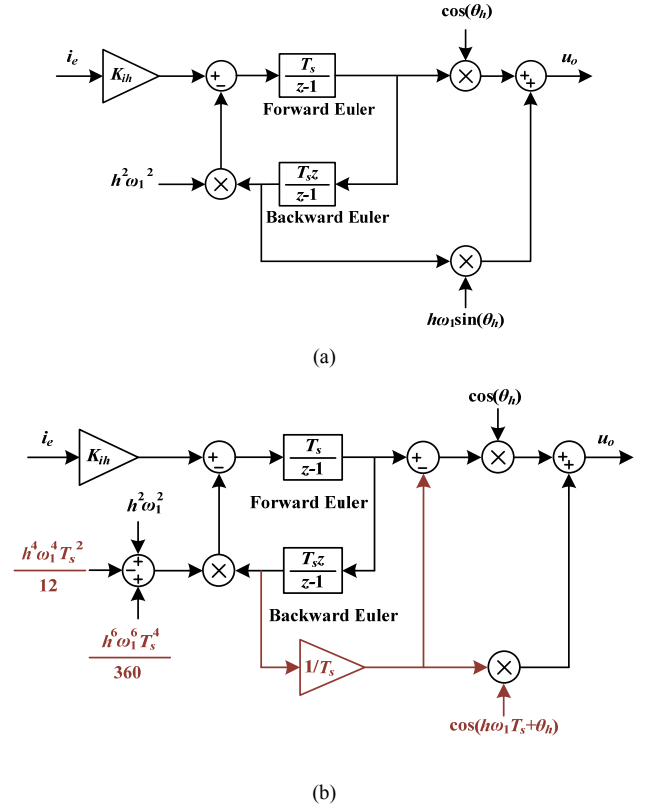


Fig. 12. Block diagrams showing (a) basic and (b) improved discretized resonant controllers with two integrators.

exacerbate as T_s and $h\omega_l$ increase [11].

$$G_{Rh}(z) = K_{ih} T_s \frac{\cos(\theta_h) - z^{-1} \cos(\theta_h - h\omega_l T_s)}{1 - 2z^{-1} \cos(h\omega_l T_s) + z^{-2}} \quad (13)$$

Fig. 12(b) therefore shows an improved resonant controller [8] with two added features for gaining better accuracy. The first is to replace $\cos(h\omega_l T_s)$ in the denominator of (13) with a higher sixth-order Taylor series to strengthen the resonant pole accuracy. The second is to modify the phase lead input θ_h so

that more accurate zeros can be obtained. The improved resonant controller generally functions well with a L -filtered converter, for which the required phase lead θ_h is readily determined. The determination of θ_h for a LCL -filtered converter is however not straightforward because of possible phase change around the LCL resonance frequency. This is further complicated by the non-minimum phase behavior of the proportional capacitor-current damper, which in principle, will restrict the compensation of higher harmonic frequency.

Fortunately, the non-minimum phase behavior can be removed by the proposed virtual RC damper, where the frequency range for harmonic compensation can hence be extended. The next subsection is thus used to identify this range, within which θ_h can be determined easily for harmonic compensation.

B. Effective Compensation Range

Figs. 8 to 10 have earlier shown the prominent reduction of gain crossover frequency, as the grid inductance increases. Consequently, the harmonic compensation range chosen must be reduced significantly, if the traditional guideline of designing resonant controllers below the gain crossover frequency is followed. More correctly, resonant controllers should be able to compensate well as long as their frequencies are below the LCL resonance, at which a rapid transition in phase occurs. The resonance frequency is therefore the true upper limit, below which, the phase lead θ_h needed for each resonant controller can be approximated as [8]:

$$\theta_h = \frac{\pi}{2} + 1.5h\omega_1 T_s \quad (14)$$

Despite that, there is a concern to note when high cutoff frequency ω_{rc} is chosen for the high-pass-filtered RC damper. The issue can be understood from Fig. 13, which is an extension of Fig. 10 for the case of $L_g = 9$ mH with different K_{rc} and ω_{rc} values chosen for the RC damper (like Fig. 10, Fig. 13 assumes a proportional grid current controller $G_c(s)$). The diagrams in Fig. 13 clearly show that to arrive at the same magnitude damping, K_{rc} needed by the larger ω_{rc} is much higher, which in turn, leads to a larger phase lag around the LCL resonance frequency.

The larger phase lag has fortunately not destabilized those plots drawn in Fig. 13(b) for a larger ω_{rc} , because of the proportional grid current controller $G_c(s)$ assumed. This is however not always true when multiple resonant controllers have been added to $G_c(s)$ for realizing selective harmonic compensation. To demonstrate, Fig. 14 re-plots Fig. 13 for two sets of K_{rc} and ω_{rc} , and with the resonant transfer functions included. Both sets of values give the same damping, but with a higher ω_{rc} and hence phase lag, the zoomed-in view in Fig. 14(b) shows a reduced PM for the 23rd and 25th resonant controllers placed near the LCL resonance. The reduced PM has, in fact, caused the phase of the 25th resonant controller to fall below -180° , which indicates an unstable 25th harmonic compensation [10], [18].

In terms of harmonic compensation stability, it is therefore

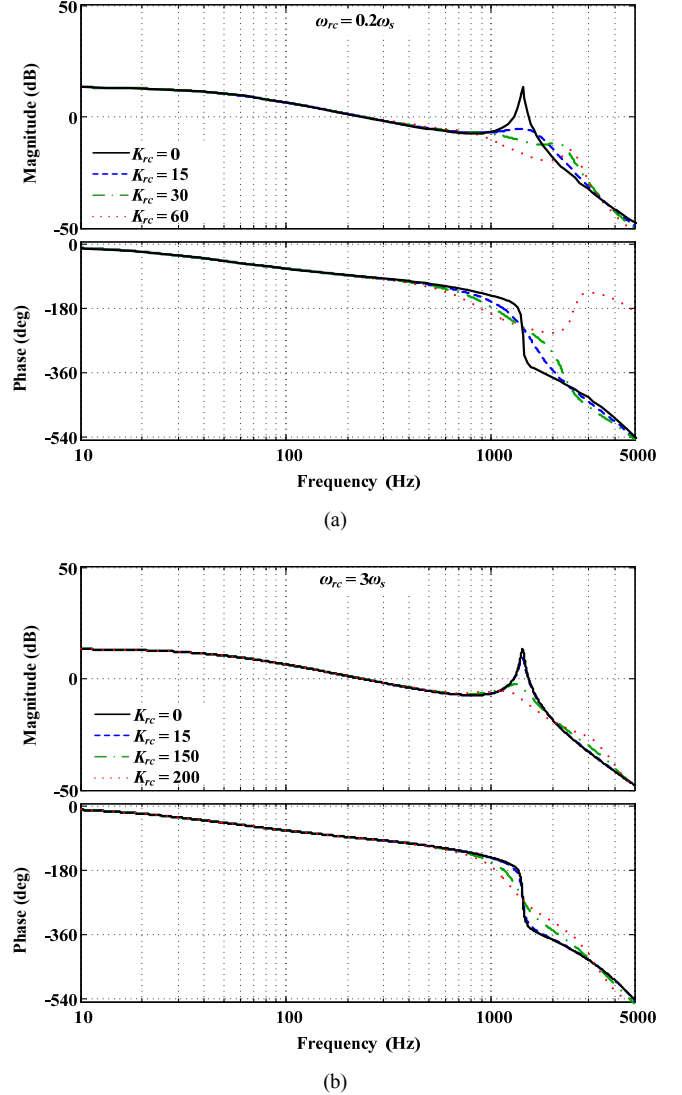
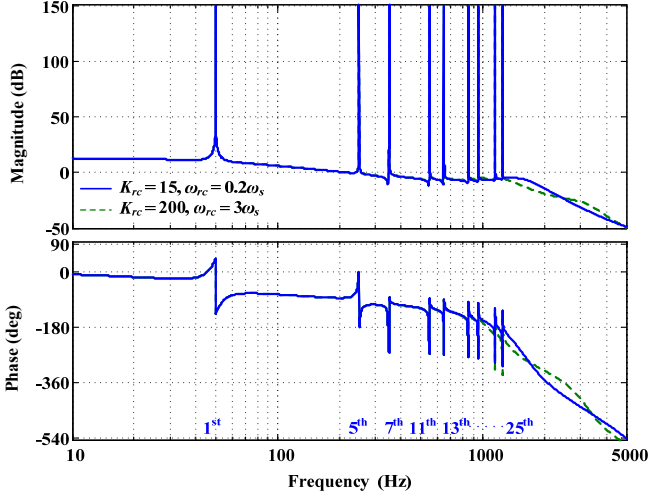


Fig. 13. Effects of (a) low ($\omega_{rc} = 0.2\omega_s$) and (b) high ($\omega_{rc} = 3\omega_s$) cut-off frequencies of the virtual RC damper around LCL resonance.

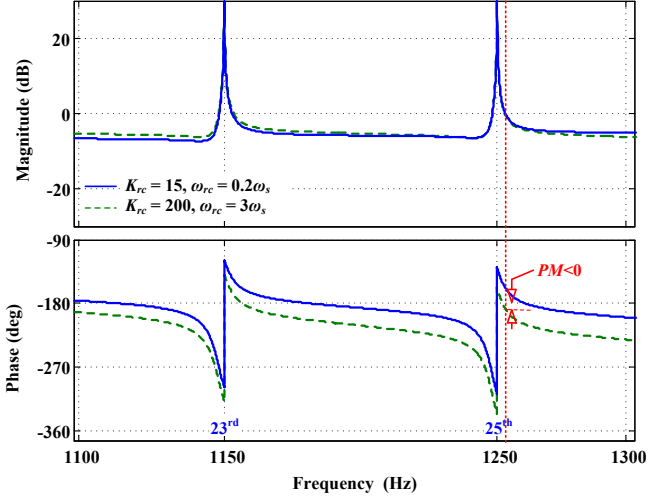
important to keep ω_{rc} low. This is however in contrast to Subsection II (B), where a higher ω_{rc} is recommended for a better damping robustness even when the grid inductance L_g varies widely. A compromised range might hence be $0.2\omega_s \leq \omega_{rc} < 0.5\omega_s$, where the upper limit denotes the Nyquist angular frequency. Generally, the Nyquist frequency should not be exceeded because of possible noise amplification associated with the high-pass filter when in a noisy environment or sampling effects found in a digitally controlled system. It is thus a critical limit that should preferably be observed in practice, even though not strictly necessary.

V. EXPERIMENTAL RESULTS

To verify the analysis presented, the LCL -filtered converter shown in Fig. 1 is implemented and connected to a *California Instruments* MX-series AC power supply for emulating the grid. Parameters chosen for the converter were listed in Table I, from which parameters summarized in Table II are designed



(a)



(b)

Fig. 14. Phase-lag effects introduced by high cutoff frequency of the virtual RC damper. (a) Full view. (b) Zoomed-in view around 23rd and 25th harmonics.

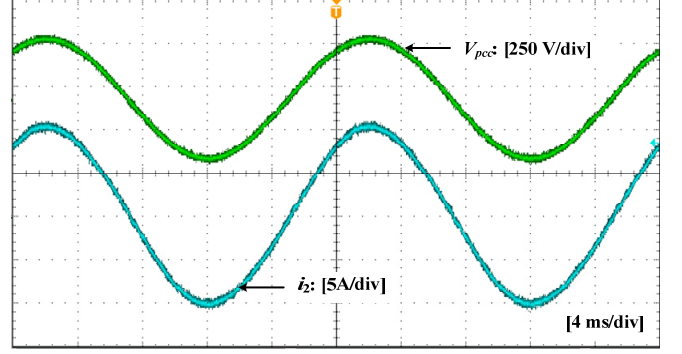
TABLE II
CONTROLLER PARAMETERS

Symbol	Meaning	Value
K_p	Proportional gain	20
K_{rl}	Fundamental resonant controller gain	800
K_{rh}	Harmonic resonant controller gain	800
K_{rc}	High-pass filter gain	15
ω_{rc}	High-pass filter cut-off frequency	$0.2\omega_s$

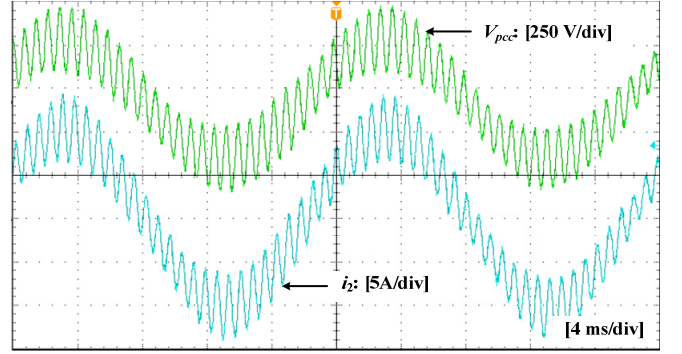
for the RC damper and resonant current controllers, following the discussion presented in the paper. The resulting control scheme is realized with a *dSPACE* DS1006 system, whose produced results are explained as follows.

A. Active Damping

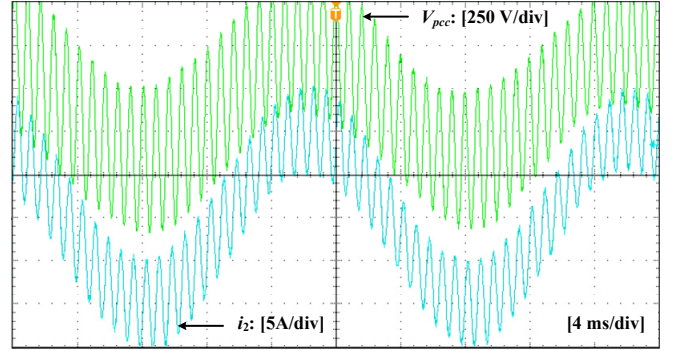
Fig. 15 shows the measured PCC voltage and grid current for one phase of the *LCL*-filtered converter with no active damping added. As the grid inductance L_g increases from Fig.



(a)



(b)



(c)

Fig. 15. Measured per phase PCC voltage and grid current without external active damping. (a) $L_g = 0$ mH. (b) $L_g = 4.5$ mH. (c) $L_g = 9$ mH.

15(a) to (c), the converter obviously becomes unstable as the *LCL* resonance frequency moves below the critical value of $f_s/6 = 1.67$ kHz. This matches the expectation deduced from Fig. 8.

Fig. 16 next shows the waveforms obtained with the proportional capacitor-current active damping added. The step response of the grid current is not effectively damped with visible oscillatory ripple noted. The oscillatory response in Fig. 16(b) is particularly more prominent, because with $L_g = 4.5$ mH, its *LCL* resonance frequency is the closest to ω_{nr} read from Fig. 6 at $\omega_{rc} = 0$. Above ω_{nr} , negative virtual resistance will be inserted unintentionally to destabilize the converter.

Fig. 17 proceeds to show the measured results with the proposed virtual RC damper added. It is clear that the system remains stable and well damped for all three tested L_g values. This is certainly in agreement with theoretical analysis.

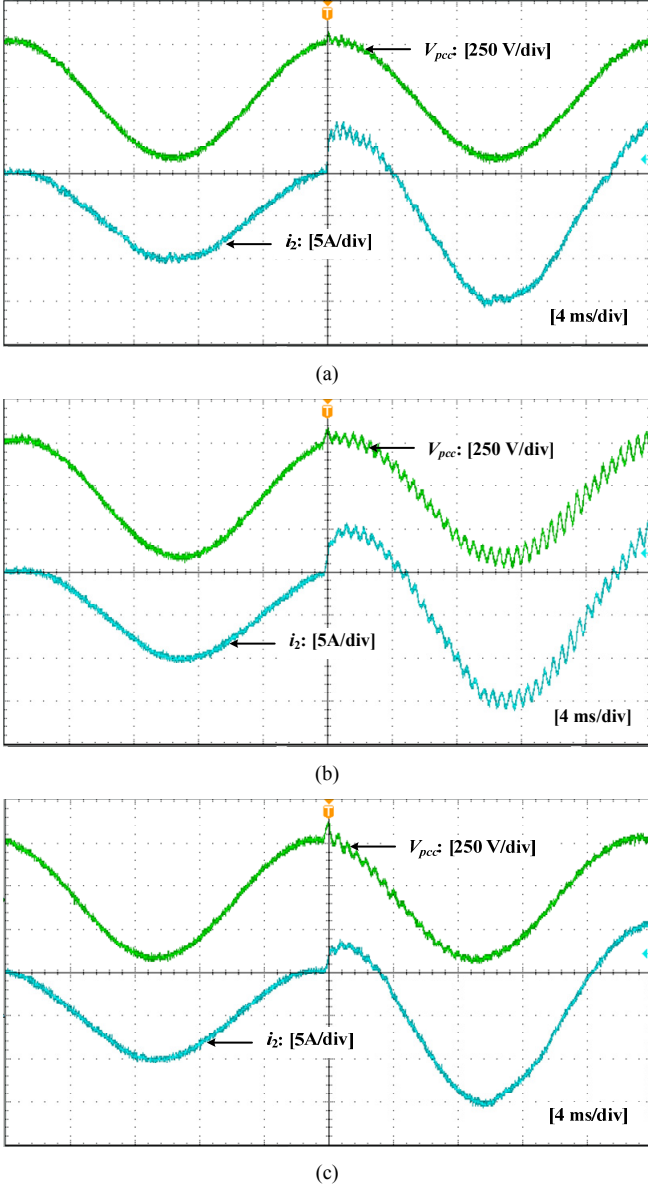


Fig. 16. Measured per phase PCC voltage and grid current with conventional proportional capacitor-current active damping. (a) $L_g = 0$ mH. (b) $L_g = 4.5$ mH. (c) $L_g = 9$ mH.

B. Selective Harmonic Compensation

For evaluating harmonic mitigation, a square PCC voltage with sizable low-order harmonics was created by the AC power supply. With an improperly controlled converter, its injected grid current will usually be non-sinusoidal with significant low-order current harmonics anticipated. These low-order current harmonics can however be eliminated by selective harmonic compensation to obtain a sinusoidal grid current even with the square PCC voltage. The purpose of the results presented in this subsection is thus to simultaneously verify harmonic compensation up to the LCL resonance (and not gain cross-over) frequency and frequency-domain analyses presented in Fig. 14, after applying the necessary RC damping proved in Fig. 17.

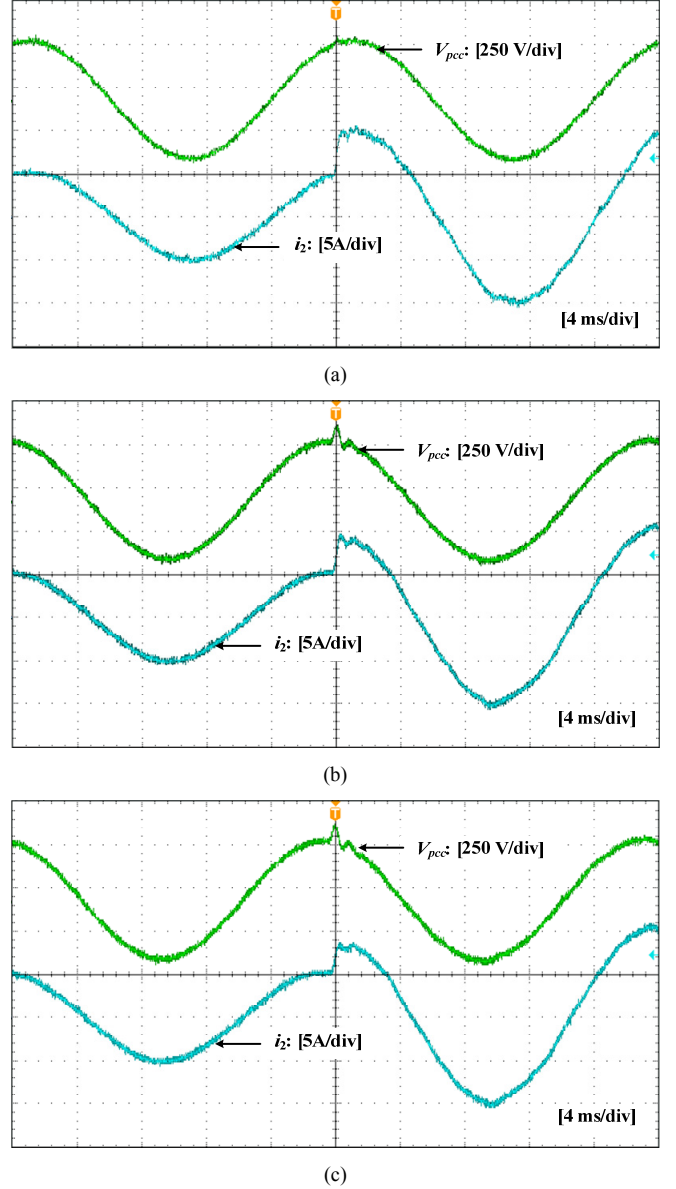


Fig. 17. Measured per phase PCC voltage and grid current with proposed virtual RC damper. (a) $L_g = 0$ mH. (b) $L_g = 4.5$ mH. (c) $L_g = 9$ mH.

Resonant controllers for the three tested grid inductances are thus placed up to the highest of 43rd harmonic for $L_g = 0$, highest of 29th harmonic for $L_g = 4.5$ mH, and highest of 25th harmonic for $L_g = 9$ mH. These highest resonant terms are all very close to their respective LCL resonance frequencies, hence allowing the objectives of the paper to be tested. The experiments are repeated twice for the two chosen cutoff frequencies of $\omega_{rc} = 0.2\omega_s$ and $3\omega_s$, similar to those used in Fig. 14.

Results obtained are shown in Figs. 18 and 19, respectively, where the latter shows more oscillatory response caused by the phase lag effect discussed in Subsection IV (B). It is therefore appropriate to tune ω_{rc} within the range of $0.2\omega_s \leq \omega_{rc} < 0.5\omega_s$ to ensure the effective harmonic compensation up to the LCL resonance frequency, while preserving robustness even when L_g varies.

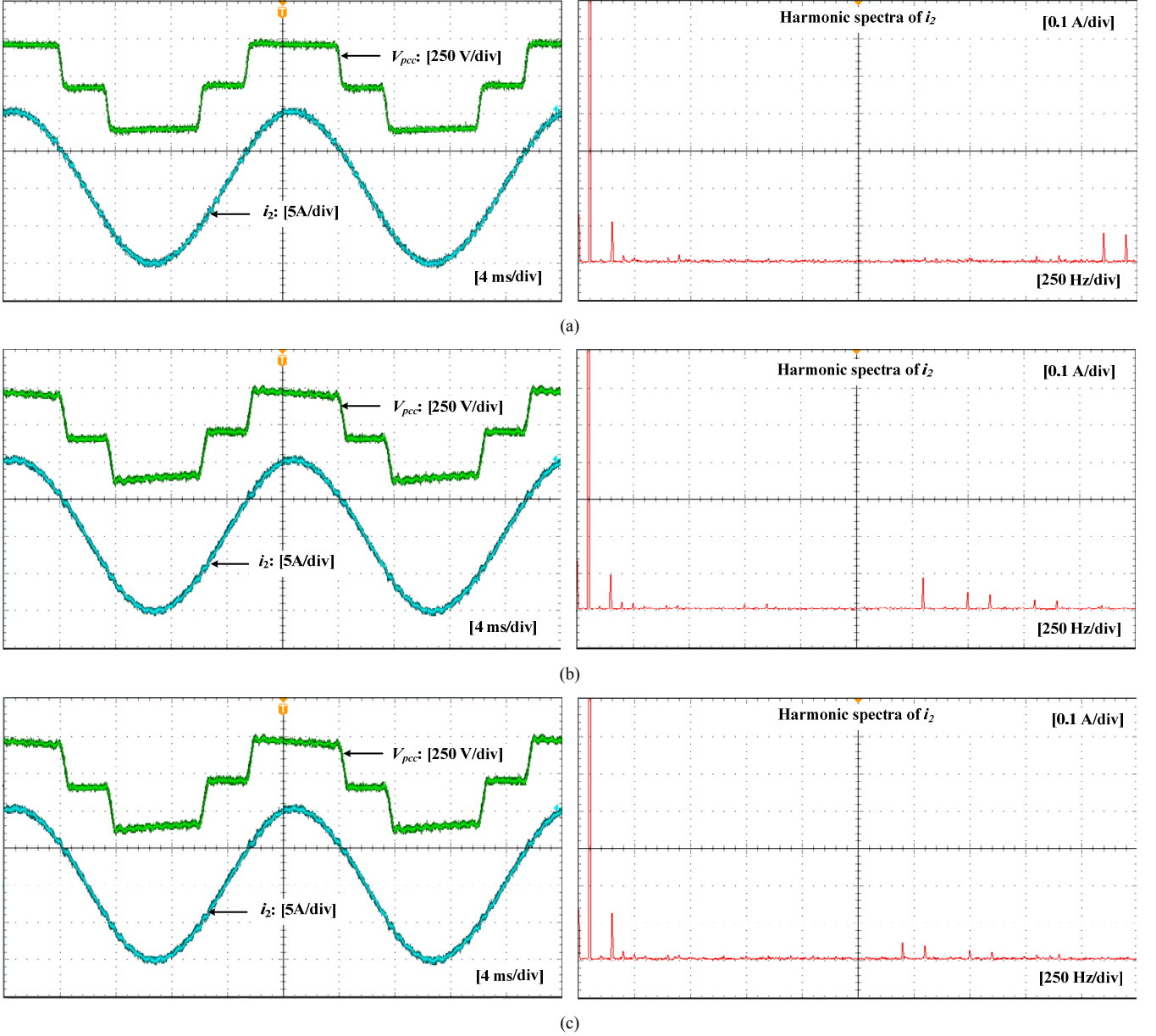


Fig. 18. Measured per phase PCC voltage and grid current with low cut-off frequency for the virtual RC damper ($\omega_{rc} = 0.2\omega_s$). (a) $L_g = 0$ mH. (b) $L_g = 4.5$ mH. (c) $L_g = 9$ mH.

VI. CONCLUSIONS

This paper presents a holistic analysis of active damping and selective harmonic compensation for LCL -filtered, grid-connected converters. Experimental results obtained show that the proposed virtual RC damper dampens LCL resonance well with the instability influences, caused by the system delays, mitigated promptly. The damped system, in turn, allows the harmonic compensation to be extended until LCL resonance, rather than the gain crossover frequency. This expectation has been verified by three experimental cases, in which the highest resonant terms have been placed close to their respective LCL resonance frequencies. Appropriate design guidelines are also given, which upon followed, results in converters with a better robustness and the less harmonics even if the grid inductance varies widely.

REFERENCES

- [1] M. Liserre, F. Blaabjerg, and S. Hansen, "Design and control of an LCL -filter-based three-phase active rectifiers," *IEEE Trans. Ind. Appl.*, vol. 41, no. 5, pp. 1281-1291, Sept./Oct. 2005.
- [2] E. Twining and D. G. Holmes, "Grid current regulation of a three-phase voltage source inverter with an LCL input filter," *IEEE Trans. Power Electron.*, vol. 18, no. 3, pp. 888-895, May 2003.
- [3] X. Wang, F. Blaabjerg, and W. Wu, "Modeling and analysis of harmonic stability in an AC power-electronics-based power system," *IEEE Trans. Power Electron.*, vol. 29, no. 12, pp. 6421-6432, Dec. 2014.
- [4] X. Wang, F. Blaabjerg, M. Liserre, Z. Chen, J. He, and Y. W. Li, "An active damper for stabilizing power-electronics-based AC systems," *IEEE Trans. Power Electron.*, vol. 29, no. 7, pp. 3318-3329, Jul. 2014.
- [5] X. Wang, F. Blaabjerg, and Z. Chen, "Synthesis of variable harmonic impedance in inverter-interfaced distributed generation unit for harmonic damping throughout a distribution network," *IEEE Trans. Ind. Appl.*, vol. 48, no. 4, pp. 1407-1417, Jul./Aug. 2012.

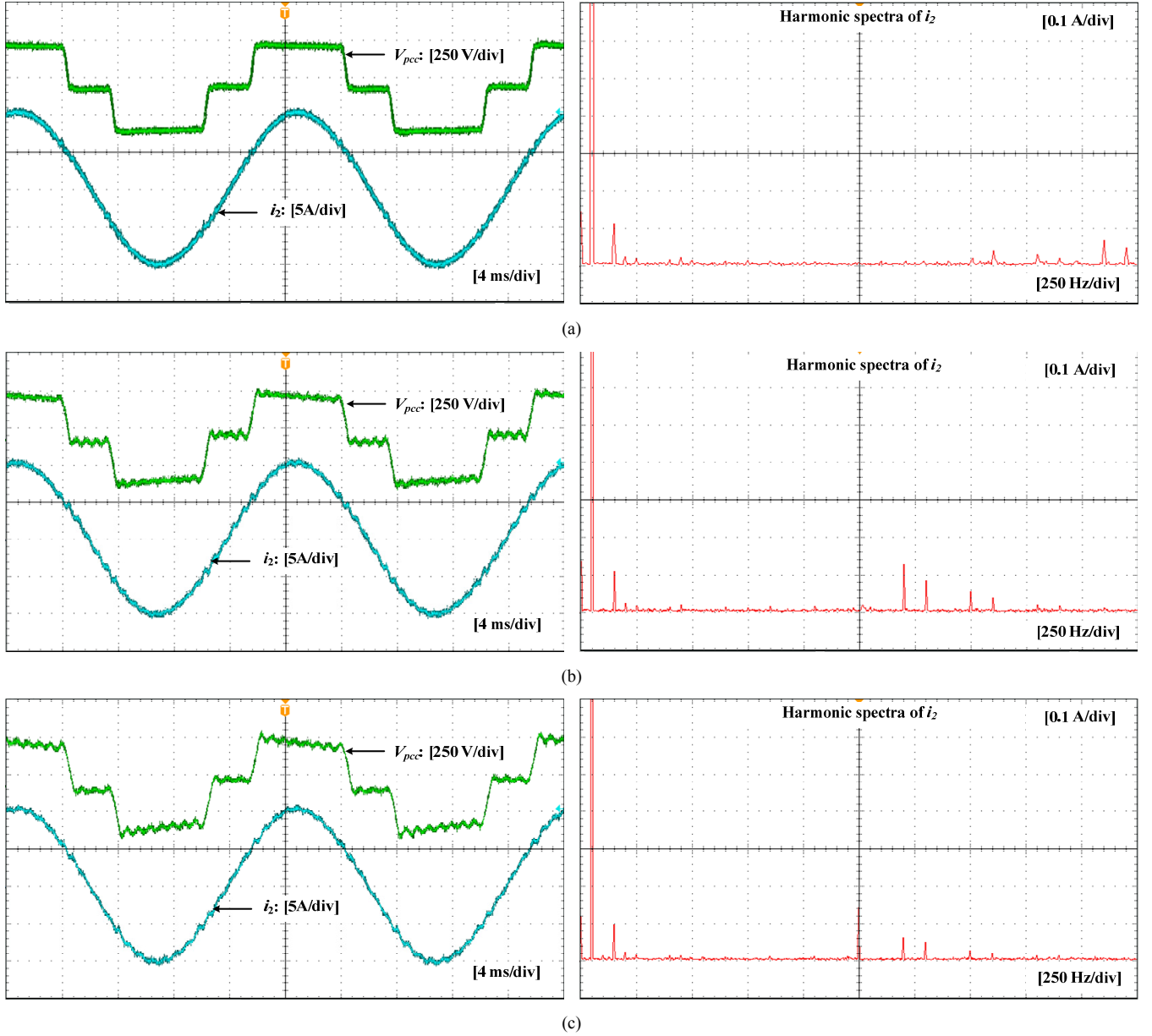


Fig. 19. Measured per phase PCC voltage and grid current with high cut-off frequency for the virtual RC damper ($\omega_{rc} = 3\omega_s$). (a) $L_g = 0$ mH. (b) $L_g = 4.5$ mH. (c) $L_g = 9$ mH.

- [6] X. Yuan, W. Merk, H. Stemmler, and J. Allmeling, "Stationary frame generalized integrators for current control of active power filters with zero steady-state error for current harmonics of concern under unbalanced and distorted operating conditions," *IEEE Trans. Ind. Appl.*, vol. 38, no. 2, pp. 523-532, Mar./Apr. 2002.
- [7] P. Mattavelli, "A closed-loop selective harmonic compensation for active filters," *IEEE Trans. Ind. Appl.*, vol. 37, no. 1, pp. 81-89, Jan./Feb. 2002.
- [8] R. Teodorescu, F. Blaabjerg, M. Liserre, and P. C. Loh, "Proportional-resonant controllers and filters for grid-connected voltage-source converters," *IEEE Proc. Electr. Power Appl.*, vol. 153, no. 5, pp. 750-762, Sept. 2006.
- [9] A. Yepes, F. Freijedo, J. Gandoy, O. Lopez, J. Malvar, and P. Comesana, "Effects of discretization methods on the performance of resonant controllers," *IEEE Trans. Power Electron.*, vol. 25, no. 7, pp. 1692-1712, Jul. 2010.
- [10] A. Yepes, F. Freijedo, O. Lopez, and J. Gandoy, "Analysis and design of resonant current controllers for voltage-source converters by means of Nyquist diagrams and sensitive function," *IEEE Trans. Ind. Electron.*, vol. 58, no. 11, pp. 5231-5250, Nov. 2011.
- [11] A. Yepes, F. Freijedo, O. Lopez, and J. Gandoy, "High-performance digital resonant controllers implemented with two integrators," *IEEE Trans. Power Electron.*, vol. 26, no. 2, pp. 563-576, Feb. 2011.
- [12] F. Wang, J. L. Duarte, M. A. M. Hendrix, and P. F. Ribeiro, "Modeling and analysis of grid harmonic distortion impact of aggregated DG inverters," *IEEE Trans. Power Electron.*, vol. 26, no. 3, pp. 786-797, Mar. 2011.
- [13] M. Liserre, R. Teodorescu, and F. Blaabjerg, "Stability of photovoltaic and wind turbine grid-connected inverters for a large set of grid impedance values," *IEEE Trans. Power Electron.*, vol. 21, no. 1, pp. 263-272, Jan. 2006.
- [14] Z. Li, Y. Li, P. Wang, H. Zhu, C. Liu, and F. Gao, "Single-loop digital control of high-power 400-Hz ground power unit for airplanes," *IEEE Trans. Ind. Electron.*, vol. 57, no. 2, pp. 532-543, Feb. 2010.
- [15] R. Venturini, P. Mattavelli, P. Zanchetta, M. Sumner, "Adaptive selective compensation for variable frequency active power filters in

- more electrical aircraft," *IEEE Trans. Aero. Electron. Syst.*, vol. 48, no. 2, pp. 1319-1328, Apr. 2012.
- [16] R. N. Beres, X. Wang, F. Blaabjerg, C. L. Bak, and M. Liserre, "A review of passive filters for grid-connected voltage source converters," in *Proc. IEEE APEC* 2014, pp. 2208-2215.
- [17] R. Pena-Alzola, M. Liserre, F. Blaabjerg, R. Sebastián, J. Dannehl and F. W. Fuchs, "Analysis of the passive damping losses in LCL-filter based grid converters," *IEEE Trans. Power Electron.*, vol. 28, no. 6, pp. 2642-2646, Jun. 2013.
- [18] J. Dannehl, M. Liserre, and F. W. Fuchs, "Filter-based active damping of voltage source converters with LCL filter," *IEEE Trans. Ind. Electron.*, vol. 58, no. 8, pp. 3623-3633, Aug. 2011.
- [19] J. Dannehl, F. W. Fuchs, S. Hansen, and P. B. Thogersen, "Investigation of active damping approaches for PI-based current control of grid-connected pulse width modulation converters with LCL filters," *IEEE Trans. Ind. Appl.*, vol. 46, no. 4, pp. 1509-1517, Jul./Aug. 2010.
- [20] V. Blasko and V. Kaura, "A novel control to actively damp resonance in input LC filter of a three-phase voltage source converter," *IEEE Trans. Ind. Appl.*, vol. 33, no. 2, pp. 542-550, Mar./Apr. 2002.
- [21] R. Pena-Alzola, M. Liserre, F. Blaabjerg, R. Sebastian, J. Dannehl, and F. W. Fuchs, "Systematic design of the lead-lag network method for active damping in LCL-filter based three-phase converters," *IEEE Trans. Ind. Infor.*, vol. 10, no. 1, pp. 43-52, Feb. 2014.
- [22] M. Malinowski and S. Bernet, "A simple voltage sensorless active damping scheme for three-phase PWM converters with an LCL filter," *IEEE Ind. Electron.*, vol. 55, no. 4, pp. 1876-1880, Apr. 2008.
- [23] S. Parker, B. P. McGrath, and D. G. Holmes, "Region of active damping control for LCL filters," *IEEE Trans. Ind. Appl.*, vol. 50, no. 1, pp. 424-432, Jan./Feb. 2014.
- [24] Y. Lei, Z. Zhao, F. He, S. Lu, and L. Yin, "An improved virtual resistance damping method for grid-connected inverters with LCL filters," in *Proc. IEEE ECCE* 2011, pp. 3816-3822.
- [25] C. Bao, X. Ruan, X. Wang, W. Li, D. Pan, and K. Weng, "Step-by-step controller design for LCL-type grid-connected inverter with capacitor-current-feedback active-damping," *IEEE Trans. Power Electron.*, vol. 29, no. 3, pp. 1239-1253, Mar. 2014.
- [26] D. Pan, X. Ruan, C. Bao, W. Li, and X. Wang, "Capacitor-current-feedback active damping with reduced computation delay for improving robustness of LCL-type grid-connected inverter," *IEEE Trans. Power Electron.*, vol. 29, no. 7, pp. 3414-3427, Jul. 2014.
- [27] V. Miskovic, V. Blasko, T. Jahns, A. Smith, and C. Romenesko, "Observer based active damping of LCL resonance in grid connected voltage source converters" in *Proc. IEEE ECCE* 2013, pp. 4850-4856.
- [28] M. Wagner, T. Barth, C. Ditmanson, R. Alvarez, and S. Bernet, "Discrete-time optimal active damping of LCL resonance in grid connected converters by proportional capacitor current feedback," in *Proc. IEEE ECCE* 2013, pp. 721-727.
- [29] L. Harnefors, M. Bongiorno, and S. Lundberg, "Input-admittance calculation and shaping for controlled voltage-source converters," *IEEE Trans. Ind. Electron.*, vol. 54, no. 6, pp. 3323-3334, Dec. 2007.
- [30] S. Buso and P. Mattavelli, *Digital Control in Power Electronics*, CA: Morgan & Claypool Publ., 2006.